RESEARCH ARTICLE   **Open Access**

Temporal variability of precipitation isotopes in Damascus, Syria — implications for regional climate change

Zuhair Kattan[1*] and Saeid Nasser[1]

Abstract

Records of stable isotopes (^{2}H and ^{18}O), deuterium excess (*d*-excess) and tritium (^{3}H) values in precipitation (P) during 1990–2022, together with long-term time series (1919–2022) of air temperature (T) and P-amount values at the Damascus station, were analysed to explore the seasonal and annual variability patterns of those parameters in P and assess the vulnerability to climate change in this area. Variation of the annual average air T values over the period 1919–1969 shows an increase gradient of $\approx +0.1$ °C/decade. However, a remarkable much higher gradient ($+0.64$ °C/ decade) is calculated for the period 1990–2022. The average P-amount value calculated for the last three decades (≈ 185 mm) was lower by ≈ 28 mm, compared to the value (≈ 213 mm), relative to the reference period (1919–1969). This significant decline in the annual P-amount value by ≈ 11–13%, accompanied by an annual heating of 0.2–0.6 °C/ decade in the annual air T, is likely the result of the climate change affecting this area. The linear relationships between annual average δ^{18}O and annual average δ^2H values versus time over the period 1990–2019 indicate increased gradients in both stable isotopes (≈ 0.3–0.5‰ and ≈ 1.1–3.2‰ per decade for δ^{18}O and δ^2H, respectively), accompanied with a decrease gradient of ≈ 0.9–1.1‰ per decade in *d*-excess values. Variability of annual ^{3}H concentrations towards low levels (< 6 TU) during the later years strongly suggests the return back towards the cosmogenic production of this radioisotope in the upper atmosphere. Information gained from this work would offer new insights to improve the understanding of the temporal variability of P isotopes and assess the risks associated with climate change on the natural water resources in the Eastern Mediterranean region.

Keywords Environmental isotopes, Precipitation, Temporal variability, Climate change, Damascus, Syria

1 Introduction

Investigation of hydrogen (^{2}H and ^{3}H) and oxygen (^{18}O) isotopes of the water molecule in current precipitation (P) is a useful approach to assess and characterize a variety of hydrological and geochemical processes with relation to the water cycle (Gat, 1996; Clark & Fritz, 1997; Criss, 1999; Mook, 2001; IAEA, 2005a; Hoefs, 2009). These isotopes are greatly studied for characterizing the global and regional scale variations (Rozanski et al., 1993; Bowen & Revenaugh, 2003) and widely applied for tracing the circulation and transport of water vapour and humid air masses in the atmosphere (Aggarwal et al., 2004; Strong et al., 2007; Pfahl & Wernli, 2008). Tritium (^{3}H), as a radioactive isotope, with a half-life of ≈ 12.32 years (Lucas & Unterweger, 2000), naturally formed by interactions between the fast cosmic rays and nitrogen atoms in the upper atmosphere (Eriksson, 1983), and anthropogenically produced by nuclear experiment programmes (Akata et al., 2011), is also widely and successfully used as a radiotracer for differentiating between old and renewable waters and estimation of groundwater residence

*Correspondence:
Zuhair Kattan
cscientific21@aec.org.sy
[1] Department of Geology, Atomic Energy Commission of Syria (AECS), Damascus, Syria

time, mostly through mathematical modelling (Zuber, 1986; Kattan, 1997a).

Information on the temporal and spatial variability of the stable isotopes (δ^2H and $\delta^{18}O$) and ^3H levels in present P are also important for investigating and modelling the surface water flow in catchment areas (Kendall & Coplen, 2001; Karim & Veizer, 2002) and characterizing the groundwater in the different systems (Gonfiantini et al., 2001; Bhat & Jeelani, 2015). Determinations of P stable isotopes are also useful to interpret the paleo-climate data archives and understanding of the past, present and future climate dynamics (Johnsen et al., 1989; Swart et al., 1993; Petit et al., 1999; Aizen et al., 2005; Klein et al., 2016).

It is well documented that the major meteorological parameters, such as air temperature (T), relative humidity (RH) and P-amount values, play certain roles in the variability of P stable isotopes (Lee & Fung, 2008; Terzer et al., 2013). This is because fractionation of the stable isotopes strongly depends on these parameters, which tend to characterize the isotopic signature of the water molecule or water vapour at its initial occurrence under different climate conditions (Majoube, 1971; Gat, 1996; Criss, 1999; Terzer-Wassmuth et al., 2021; Vystavna et al., 2021). Therefore, it is chiefly important to understand the role of such parameters on the temporal and spatial variability of P stable isotopes, especially to better reconstruct the different climatic parameters in the different environments and assess the provenance of water and its modification processes in the various aquatic systems (Clark & Fritz, 1997; Leketa & Abiye, 2020).

However, the chief role is still the change in air T values (Rozanski et al., 1993) and in a second step the cause so-called P-amount effect (Risi et al., 2008). Hence, the isotopic composition of P during the cold periods is usually depleted in heavy stable isotopes while more enriched in the warmer seasons (Angert et al., 2008; Akers et al., 2017). The rain falling over higher elevation areas is steadily more depleted compared to lower elevation areas (Liu et al., 2010). Further inland, this composition is very sensitive to oscillation in air T values (Rozanski et al., 1993) whereas weakly dependent on this parameter in coastal areas (Hendricks et al., 2000). Evaporation of the rainwater drops during their falling on the ground often involves enrichment in the heavy stable isotopes (Scholl et al., 2009), and thus, any change in P isotopes because of secondary evaporation may mask the original isotopic signature of the single rainstorms (Liotta et al., 2008). In temperate regions, variations of P stable isotopes can frequently be correlated with the mean surface air T values (Aggarwal et al., 2012), whereas in equatorial zone rainfall, this relationship is almost feeble and thus unsuitable for monthly or seasonal predictions (Allen et al., 2019).

The "amount effect", which defines the tendency of stable isotopes to become more depleted with increasing P-amount values (Dansgaard, 1964; Rozanski et al., 1993), is generally not yet enough clear and mostly not consistent because of some superimposed processes, such as moisture recycling, orographic rainout and secondary evaporation (Yang et al., 2019; Vystavna et al., 2021; Mahindawansha et al., 2022). Based on studies conducted in tropical areas, it is revealed that this effect is the major controlling factor (Cruz et al., 2005). Also, it was shown that the amount effect is significant during the monsoon season (Li et al., 2022), and that variations of P stable isotopes can even occur within extreme short time during the single rainstorms (Munksgaard et al., 2012). In all cases, the effects of air T- and P-amount on P stable isotopes are reflected by linear relationships over long-term monitoring periods. Thus, studying the temporal variability of P isotopes during long-time periods would give more in-depth details on the potential regional and global climate changes (Rozanski et al., 1992; Terzer-Wassmuth et al., 2021).

Assessments of the regional climate change in the Mediterranean region have shown that this region is expected to be affected strongly by the increased regional warming (Mariotti et al., 2015). Over the twentieth century, this region will be subjected to strong warming in summer and typically lower rainfall in winter (Giorgi & Lionello, 2008; Ozturk et al., 2015). According to Önol and Semazzi (2009), the seasonal surface air T averages in Syria during 2071–2100 will rise by 2.8 °C and 4.4 °C in winter and autumn, respectively, relative to the period (1961–1990). This increase in climate warming will be accompanied by decline in the seasonal P-amount averages by −28.8% and −18.6% in winter and spring, respectively, and an increase of +4.9% and +90.5% in summer and autumn, respectively. The annual P-amounts are expected to decline by 5–25% during 2040–2069 and 5–30% during 2070–2099, relative to the period (1961–1990), together with a significant rain shortage (24–32%) in winter (Lelieveld et al., 2012).

The effect of climate change at the daytime regional warming (3.5 °C) will considerably amplify the rainfall deficit and thus increasing the risks of drought occurrences in Syria (Guiot & Cramer, 2016; Lehner et al., 2017). A shifting from 1.5 to 2 °C in the regional warming will be reflected in strong increases in dryness and decreases in water availability, likely the renewable waters (Davis et al., 2017). Hence, as Syria is situated in an arid to semiarid region, and severely subjected to extensive changes in its climate under increased warming, the expected substantial future decrease in rainfall will result in high risks to the natural ecosystems, national human

activities and country economy (Smiatek et al., 2013; Kelley et al., 2015).

This paper, which aims primarily to characterize the seasonal and annual variability patterns of P isotopes in the Damascus rainfall, has the following main objectives: (1) characterizing the isotopic signatures of P at this station during a period of 22 years, (2) quantifying the temporal variations of P isotopes and exploring the controls of the meteorological parameters on variability of these isotopes, and (3) assessing the vulnerability to climate change in this area. Implications for the regional climate change were extracted by analysing concurrently the linear relationships between annual average and annual amount-weighted means (AWM) values of P isotopes over time, as well as the variability of the meteorological parameters during long-term periods.

2 Methods

2.1 Site description

The station selected for rainwater (RW) sampling is situated on the roof of Soumaria building, located to the west of the Damascus city, the capital of Syria (Fig. 1). The geographical coordinates for this station are as follows: 36.10°E, 33.35°N and ≈675-m elevation (H) above the sea level. This station, nearly placed in a flat plain area at distance of ≈80 km from the Mediterranean Sea (MS), is surrounded by several high elevated structures, such as the Mt. Hermon (2814 m), Mt. anti-Lebanon (2466 m), Mt. Al-Arab (1790 ml) and the southern Palmyrides series (up to 1308 m), situated close to the Syrian Desert ($H < 600$ m).

The weather in Damascus is influenced by a Mediterranean type of climate, with warm to hot and dry summers and moderate rainy winters (Meslmani et al., 2010). The annual average air T values range between 16.3 ± 7.6 °C (Euroweather) and 18.4 ± 6.0 °C (stat.world), while annual average RH values vary between $50 \pm 14\%$ and $56 \pm 13\%$ (climatemps.com; NOAA). Analysis of the wind trends in the Damascus area shows that the major prevailed winds (≈75%) were coming from the south, southwest and west directions (weatheronline.co.uk).

The rainy season in Damascus is usually short, extending from November to May, with a completely dry period from June to August. The opportunity for occurring light rain showers in September and October is also possible. The number of the rainy days in Damascus (19–68) is usually much higher than the snowy (≈11) days (weather–atlas.com). The distribution of annual average P-amount values in southern Syria shows a gradual increase from east to west, from < 100 mm in the Syrian Desert up to 800 mm on the Mt. Hermon summit (Fig. 2).

2.2 Precipitation sampling

RW sampling from the Damascus-Soumaria station was started in December 1989. The datasets belonging to this study cover three monitoring periods (December 1989 to April 1993, December 2003 to April 2006 and October 2007 to March 2022). The data of the first two periods (up to April 2006) refer to samples collected as a monthly mixture, whereas those of the last period (2007–2022) refer to samples collected either as daily (single rainstorms) or monthly composite (mixture) samples. A total of 224 daily and 95 monthly composite samples were collected during this study. Only 2 daily samples were collected in summer (June and August).

Daily sampling is based on systematic collection twice a day (morning and evening), whereas monthly sampling is made by accumulating the daily P-amounts, and
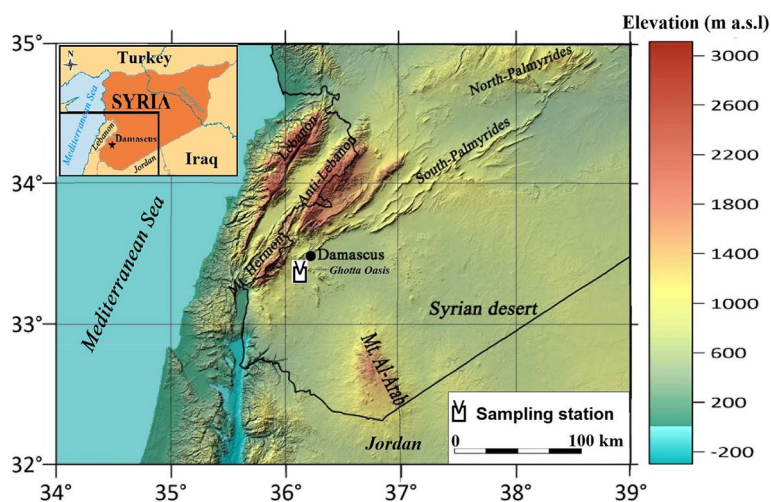

Fig. 1 Location map of south-western Syria showing the main topographical structures and site of P sampling
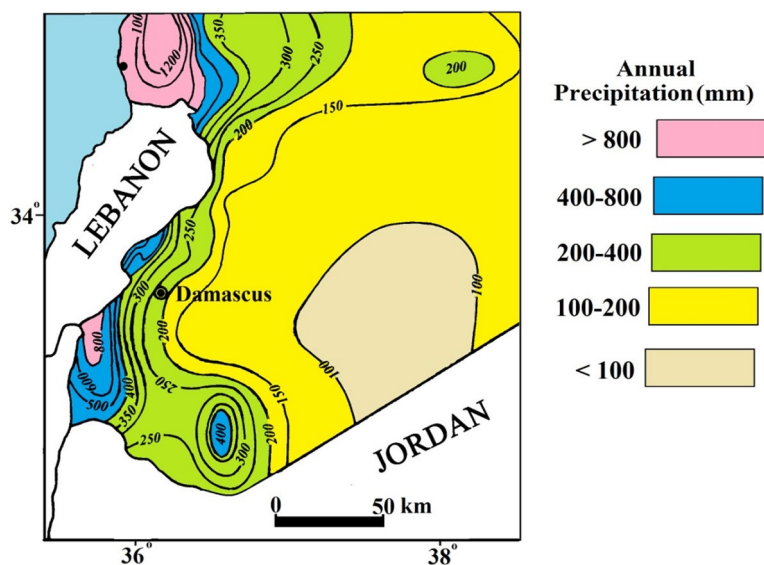
Fig. 2 Distribution of annual P-amounts in south-western Syria

storing all quantities collected during the entire month in a tightly sealed container, large enough to contain the month P-amount. Both daily and monthly samples were promptly kept in a special refrigerated room ($T < 5$ °C) until the time of analysis.

A simple dish funnel (diameter ≈80 cm) designed to fit with the frequent P-amounts at the Damascus area was used for P collection. This funnel is securely connected to a plastic container of 20 L, by using a plastic tube wrapped several turns inside the container to prevent from water evaporation. A simple stainless steel rain gauge device (precision ≈0.1 mm) was used for P-amount measurements.

2.3 Isotopic analyses

Two rinsed glass or polyethylene bottles were filled for conducting the isotopic analyses of RW samples. A small bottle of 50 mL was filled for the determination of the stable isotope ratios ($\delta^{18}O/\delta^{16}O$ and δ^2H/δ^1H), for which the subsequent analyses were conducted by using a Finnigan Mat mass spectrometer, with measurement accuracy better than ± 0.1‰ and ± 1.0‰, for $\delta^{18}O$ and δ^2H, respectively. The Vienna Standard Mean Ocean Water (VSMOW) and the Greenland Ice Sheet Precipitation (GISP) standards, carefully prepared and widely distributed by the International Atomic Energy Agency (IAEA), were used for calibrating the analytical results of $\delta^{18}O$ and δ^2H ratios (Gonfiantini, 1978; Coplen, 1996).

A second bottle of 1 l was also filled for ^3H determination, precisely when the P-amounts collected were sufficient to conduct this analysis. The subsequent ^3H analyses were performed, after electrolytic enrichment

of the RW samples, by using a liquid scintillation counter with detection limit below 0.5 TU (1 TU is equal to 1 ^3H atom per 10^{18} atoms of ^1H). More information on P sampling and analytical procedures of these isotopes were given by Kattan (2019).

Quality assurance procedures, relative to the ISO/IEC 17025 system, are strictly applied in all laboratories of the Atomic Energy Commission of Syria (AECS), and validity of the analytical results is verified by participation in the diverse inter-comparison tests, organized by either the IAEA (WICO and TRIC), or other regional authorities.

2.4 Statistical analysis and calculations

The softwares Excel 2007 and StatView 5 were used for conducting the descriptive statistics (min, max, mean, standard deviation (SD) and median) of isotopic and meteorological data.

Measured ratios of the stable hydrogen (^2H) and oxygen (^{18}O) isotopes in the RW samples were expressed in the δ notation (‰), relative to VSMOW, defined as follows:

$$\delta = [(R_{sam} - R_{std})/R_{std}] \times 1000 \tag{1}$$

where R_{sam} and R_{std} refer to the ratio ($^2H/^1H$ or $^{18}O/^{16}O$) in the samples and VSMOW standard, respectively.

The deuterium excess (*d*-excess or *d*) value in the RW sample was calculated by applying the Dansgaard (1964) formula, defined as follows:

$$d - excess = \delta^2H - 8\delta^{18}O \tag{2}$$

The AWM value that considers the "P-amount effect" on the isotopic composition during any monitoring

period (weeks, months or years) was calculated by using the formula of Yurtsever and Gat (1981):

$$AWM = \sum_i^n (P_i \times C_i) / \sum_i^n (P_i) \qquad (3)$$

where P_i is the daily or monthly P-amount value and C_i is the isotopic composition of RW sample for the period i (days or months).

As the standardised P index (SPI) is a statistical marker largely used for the assessment of drought stress, mostly the wetter and drier climate time series, this index was computed using the following equation (Angelidis et al., 2012; Sarker et al., 2021).

$$SPI = \frac{Pi - Pm}{\sigma} \qquad (4)$$

where Pi is the annual P-amount of year i, Pm is the long-term mean annual P-amount value and σ is the SD of annual P-amounts.

In order to identify similarities and compare between the time-series variability results of the meteorological and isotopic data, the paired *t*-test analysis was carried out using the software StatView 5 by adapting the hypothesized mean difference of 0 and confidential interval of 95% (Bevans, 2022).

3 Results and discussion

3.1 Variability of stable isotopes in RW samples

To identify the variability of the stable isotopes ($\delta^{18}O$, δ^2H) and *d*-excess values in the daily and monthly RW samples collected at the Soumaria station during the period 2007–2022, a detail descriptive statistic was performed (Table 1). Accordingly, the stable isotope ratios in the daily samples varied from −16.6 to +4.1‰ and from −116 to +30‰, with average values of −5.3±3.5‰ and −29±25‰ for $\delta^{18}O$ and δ^2H, respectively. These isotopes changed in the monthly composite samples from −12.7 to +2.7‰ and from −80 to +29‰, with average

values of −5.5±3‰ and −31±20‰ for $\delta^{18}O$ and δ^2H, respectively. Thus, the spread in isotope ratios in the daily samples is greater compared to the monthly samples. However, both ranges are rather comparable to the ranges (−14.6 to +7.4‰ and −101 to +35‰ for $\delta^{18}O$ and δ^2H, respectively), previously determined in the RW samples collected all over Syria during the period 1990–2006 (Kattan, 2019).

The variability of *d*-excess values in both daily and monthly samples is rather similar, varying from <0‰ in the samples highly evaporated or originated from hot and dry sources, up to 27–30‰ in the samples strongly affected by exchange with the enriched moisture ($d \approx 30‰$), produced from the MS (Gat et al., 2003). Both ranges are also identical to the range (<0 to +30‰), previously reported for the *d*-excess values in the Syrian rainfall (Kattan, 2019).

The average *d*-excess values in the daily and monthly samples are rather identical (13±8‰), and both are lower than the value (22‰), given by Nir (1967) for the Mediterranean meteoric water line (MMWL). The AWM $\delta^{18}O$ and AWM δ^2H values are constantly lower than the average and median $\delta^{18}O$ and δ^2H values, likely as the isotopic composition of P associated with high rain events ($p > 10$ mm) is usually much depleted compared to low rain events. Oppositely, the AWM *d*-excess value (15–16‰) in both daily and monthly samples is higher by ≈1–3‰ compared to the median and average *d*-excess values. The average *d*-excess and AWM *d*-excess values (15±9‰ and 19±1‰, respectively), previously calculated in the monthly composite samples collected at the Damascus station (Kattan, 2019), were much closer to the value (22‰), given by Nir (1967).

3.2 Variability of tritium in RW samples

The descriptive statistics of ^3H concentrations in the monthly RW samples collected at Damascus during the period from December 1989 to May 2019 are shown in

Table 1 Descriptive statistics of environmental isotope values in the daily and monthly composite RW samples collected at the Damascus-Soumaria station during the period 2007–2022

Parameter	Type of data	Statistics					
		Min	Max	Average	SD	Median	AWM
$\delta^{18}O$ (‰)	Daily	−16.6	4.1	−5.3	3.5	−5.6	−7.1
	Monthly	−12.9	2.7	−5.5	3.0	−5.5	−6.7
δ^2H (‰)	Daily	−116	30	−29	25	−29	−41
	Monthly	−80	29	−31	20	−33	−39
d-excess (‰)	Daily	<0	30	13	8	15	16
	Monthly	<0	27	13	7	14	15
^3H (TU)	Monthly	1.9	14.9	4.8	2.6	3.9	4.5

Table 1. The concentrations of ^{3}H varied in the range from 1.9 to 14.9 TU, with an average value of 4.8 ± 3.6 TU, slightly higher than the median (3.9 TU) or the AWM (4.5 TU) ^{3}H values. The current ^{3}H average is thus higher by ≈ 1.1 TU compared to the value (5.9 ± 3.5), previously calculated as an average value for the period 1989–2006. This difference clearly means that the concentration of ^{3}H in current P is mostly due to the natural cosmogenic production of this radioisotope in the upper atmosphere before the start of the nuclear weapons tests (Eriksson, 1983). Previous assessments of spatial distribution of ^{3}H content in the rainfall in this region showed a build-up in ^{3}H values with increasing distance from the MS coast, likely because of the continuous mixing between the low ^{3}H moisture produced from the MS and the high ^{3}H moisture derived from the inland areas (Gat & Carmi, 1970; Kattan, 1997b, 2021).

3.3 Local meteoric water line

In order to define the commonly so-called local meteoric water line (LMWL), the relationships between δ^2H and δ^{18}O values in the daily and monthly composite RW samples collected at the Soumaria station during the period 1990–2022 were determined (Fig. 3). Distribution of the sample points in this graph permits to observe that all the sample points are distributed between two lines: the global meteoric water line (GMWL), defined by Craig (1961) as δ^2H$=8\delta^{18}$O$+10$, and the MMWL, given by Nir (1967) as δ^2H$=8\delta^{18}$O$+22$. Most of the sample points representing the depleted isotopic ratios are rather scattered close to the MMWL, while those representing the enriched or evaporated samples are located close to the GMWL. All samples fit nicely with a least squares regression line and defines the so-called LMWL, approximated by the following equations:

$$\delta^2\text{H} = (6.77 \pm 0.14)\delta^{18}\text{O} + (6.8 \pm 0.9) \qquad (5)$$

with [$R^2 = 0.93$, p-value < 0.0001 and $N = 224$] for the daily data, and

$$\delta^2\text{H} = (6.68 \pm 0.20)\delta^{18}\text{O} + (5.8 \pm 1.3) \qquad (6)$$

with [$R^2 = 0.94$, p-value < 0.0001 and $N = 95$] for the monthly data.

The line slope values for daily and monthly data (≈ 6.7–6.8) are rather similar and lower than the value 8, determined for the isotopic fractionation under equilibrium condition (Craig, 1961; Rozanski et al., 1993). The sample points representing the most depleted isotopic ratios match remarkably with a line slope of ≈ 8. These samples can isotopically be considered as slightly or not affected by evaporation. However, as the re-evaporation of the raindrops is usually associated with a line slope
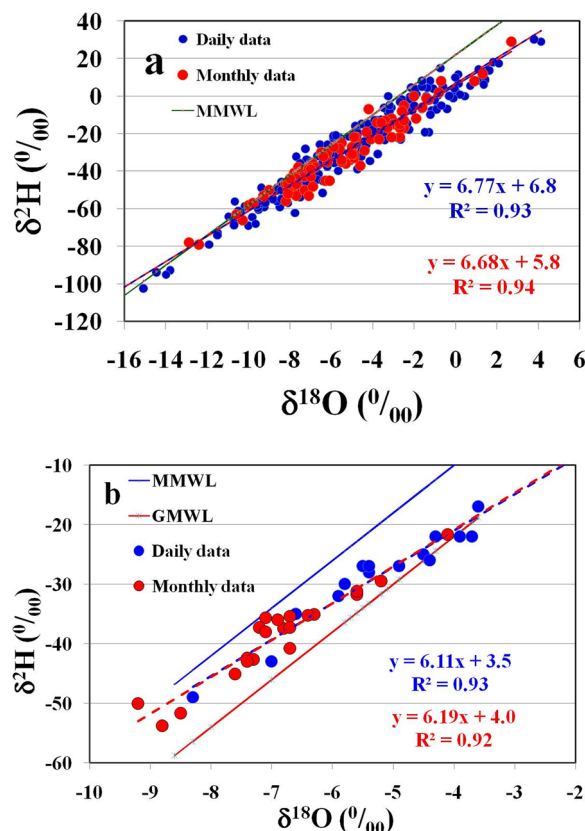

Fig. 3 The relationships between δ^2H and δ^{18}O values in daily and monthly RW samples (**a**) and between annual average δ^2H and annual δO values (daily data) and annual AWM δ^2H and annual AWM δ^{18}O values (monthly data) in the RW samples (**b**) collected at the Damascus station during 1990–2022

value lower than 8, the sample points scattering around a line with a slope lower than 8 means that the isotopically enriched samples (δ^{18}O > -4‰ and δ^2H > -20‰) were subjected to evaporation during their falling on the land surface (Managave et al., 2016). The line slope values calculated for the relationship δ^2H-δ^{18}O at each month of the rainy season (Table 2), varied from $\approx 6.3 \pm 1$ (May) up to $\approx 7.3 \pm 0.2$ (January). The line slope values calculated for the months from December to March are higher than 7, whereas those for the remaining months are lower (≈ 6.3–6.8), meaning thus that the rainfall in winter is less affected by evaporation, compared to those falling in spring and autumn.

The relationships (δ^2H-δ^{18}O), established on the basis of annual average values (daily data) and annual AWM values (monthly data) for the diverse rain seasons (22 years), permit to observe a different scatter between the distribution of the points representing daily and monthly data (Fig. 3b). The points representing the monthly data reflect generally more depleted isotopic ratios compared to those of the daily data. Although this

Table 2 Regression parameters of the relationship δ^2H-δ^{18}O calculated for the Damascus rainfall at each month of the rainy season

Type of data	Slope	Y-intercept	R^2	N	P-value
October	6.47 ± 0.34	4.52 ± 1.44	0.97	13	< 0.0001
November	6.46 ± 0.38	6.17 ± 1.94	0.91	31	< 0.0001
December	7.00 ± 0.30	9.95 ± 2.00	0.94	40	< 0.0001
January	7.28 ± 0.23	12.24 ± 1.82	0.96	46	< 0.0001
February	7.13 ± 0.31	9.22 ± 2.19	0.93	41	< 0.0001
March	7.17 ± 0.35	5.50 ± 2.18	0.94	30	< 0.0001
April	6.78 ± 0.72	4.67 ± 3.05	0.88	15	< 0.0001
May	6.29 ± 1.02	4.30 ± 4.03	0.91	7	0.0035
All daily data	6.78 ± 0.12	6.77 ± 0.76	0.94	224	< 0.0001
All monthly data	6.67 ± 0.19	5.66 ± 1.21	0.94	95	< 0.0001
Annual average (daily data)	6.11 ± 0.48	3.5 ± 2.6	0.93	15	< 0.0001
Annual AWM (monthly data)	6.19 ± 0.46	4.0 ± 3.2	0.92	22	< 0.0001

difference is between daily and monthly data, all points representing both data fit nicely with two least squares regression lines having nearly a similar line slope and an identical *Y*-intercept value, as approximated by the following equations (Fig. 3b):

$$\delta^2\text{H} = (6.11 \pm 0.48)\delta^{18}\text{O} + (3.5 \pm 2.6) \quad (7)$$

with [$R^2 = 0.93$, *p*-value < 0.0001 and $N = 15$] for daily data, and

$$\delta^2\text{H} = (6.19 \pm 0.46)\delta^{18}\text{O} + (4.0 \pm 3.2) \quad (8)$$

with [$R^2 = 0.92$, *o*-value < 0.0001 and $N = 22$] for monthly data.

When comparing the isotopic ratios of P collected in daily or monthly composite samples with those calculated as annual average or annual AWM isotopic values for the different rain seasons, the line slope values in the case of annual average and annual AWM values are always lower than the line slopes calculated on the basis of all samples (Table 2). The differences that were found between the two methods, precisely in the line slope ($\approx$0.5–0.7) and the *Y*-intercept value ($\approx$1.8–3.3‰), generally mean that the annual average and annual AWM values conjunctly reflect the effects of P-amount and re-evaporation of raindrops during their falling. In all cases, the line slope values estimated for the relationship δ^2H-δ^{18}O in this study (6.1–7.3 ± 1) completely agree with the slope values reported for the rainfall in the Eastern Mediterranean region, changing from 5.48 for the Bet-Dagan station (H≈36 m), the unique station that belongs to the Global Network of Isotopes in Precipitation (GNIP) in

this region (IAEA-WMO, 2021), up to 7.3 ± 0.4 for the Arneh station (H ≈1440 m), located in Syria (Kattan, 2019). The line slope values calculated also fit with the range (6.2–6.6), previously reported for the LMWLs in Jordan (Bajjali, 2012), Lebanon (IAEA, 2005b), and Syria (Abou Zakhem & Hafez, 2007).

3.4 Seasonal variability of meteorological parameters

With the aim to study the seasonal variability of the key meteorological parameters (P-amount, air T, and RH) recorded at the Soumaria station during the period 1990–2022, the monthly averages and SD values (±) for these parameters were calculated (Table 3). The highest monthly average P-amount values (>30 mm) usually occur during the period from November to February (Fig. 4a). December is the most humid month ($p > 40$ mm), while October and April are the less wet ($p < 20$ mm). However, the month of May showed an unusually high monthly average P-amount ($\approx$34 ± 32 mm), specifically because of the intensive rain events ($\approx$70 mm) occurred in May 2018. The monthly average P-amount values calculated for the months of May, October, November, and December are clearly higher than the long-term average monthly values reported for these months (climatemps.com). The monthly average P-amount values that were recorded for the period from January to March are remarkably lower than the long-term average values, reported for these months (Fig. 4a). The decrease of P-amount in winter and its increasing in autumn is likely because of the intense climate change affecting this area.

Variations in the monthly average air T values during the rainy season clearly show that the values calculated during this study are systematically higher than the long-term average monthly values (Fig. 4b), reported for the Damascus region (stat.world). The difference in the air T value during the period from January to April, compared to the long-term average values, is rather high (> 3 °C), whereas it is much lower in remaining months. The seasonal variations in the monthly average air T values are frequently marked by low T values (< 15 °C) during the period from December to March and higher T values (> 15 °C) during remaining months. The monthly average air T values in May and October are usually the highest (> 20 °C).

The seasonal variation in the average monthly RH values is reflected by remarkably high RH values (> 60%) during the period from November to February and lower values (35% < RH < 55%) during remaining months (Fig. 4c). The highest monthly average RH values are associated with the wettest months (December and January), whereas the lowest values (< 55%) usually occur at the beginning (October) and at the end of the rainy

Table 3 Monthly averages and SD ($\pm$) values of P-amount, air T, RH, δ^{18}O, δ^2H, *d*-excess and ^{3}H values in the daily and monthly RW samples collected at the Damascus-Soumaria station during the period 1990–2022

Parameter	Type of data	October	November	December	January	February	March	April	May
No. of samples	Daily	13	31	40	47	41	30	15	7
	Monthly	7	9	18	18	15	12	13	3
P-amount (mm)	Daily	8±18	8±7	11±15	12±13	9±9	6±8	7±6	17±21
	Monthly	17±25	33±20	44±36	35±22	31±18	22±15	16±18	34±32
Air T (℃)	Daily	16.4±5.7	11.1±4.0	8.8±4.3	5.2±4.6	5.5±4.0	8.4±3.7	10.3±4.3	20.8±8.5
	Monthly	20.0±1.6	17.3±2.0	12.2±4.0	12.7±4.7	13.7±5.1	15.7±4.1	20±3.3	21.5±4.6
RH (%)	Daily	66±16	78±13	82±10	81±10	78±10	70±13	64±18	46±22
	Monthly	54±6	68±7	69±10	69±8	65±10	55±6	47±12	38±5
δ^{18}O (‰)	Daily	−2.6±3.4	−3.2±3.2	−5.9±3.0	−7.0±3.9	−6.4±3.0	−5.0±3.7	−3.7±2.2	−3.3±2.4
	Monthly	−2.9±2.0	−4.6±2.3	−7.0±2.7	−7.7±2.4	−6.5±2.5	−5.4±1.6	−2.5±4.1	−3.1±4.3
δ^2H (‰)	Daily	−13±22	−32±21	−34±21	−38±29	−37±22	−30±28	−20±16	−16±16
	Monthly	−15±14	−21±15	−39±22	−44±17	−36±17	−32±9	−15±32	−18±31
d-excess (‰)	Daily	9±6	16±6	15±6	17±7	15±6	10±8	9±6	10±6
	Monthly	8±7	15±7	17±6	17±5	16±6	11±7	6±3	6±4
^{3}H (TU)	Daily	5.6±1.6	5.9±1.7	6.1±1.9	4.7±1.2	4.2±1.0	7.2±0.7	15.5±1.0	6.5±1.5
	Monthly	3.7±1.1	3.8±1.3	3.9±1.7	3.5±1.4	4.7±2.0	4.8±1.3	9.1±3.5	10.2±2.6

season (April and May). The monthly average RH values recorded within this study for the period from December to May are distinctly lower than the long-term monthly average values reported for this parameter for the same period (weatheronline.co.uk), while they are higher in October and November (Fig. 4c). The variations of the diverse meteorological parameters agree well with the strong regional warming and the typically lower rainfall in winter expected for this region as a result of climate change (Giorgi & Lionello, 2008; Ozturk et al., 2015).

3.5 Seasonal variability of P isotopes

The seasonal variations in the monthly average δ^{18}O and δ^2H values, calculated on the basis of daily and monthly data (Table 3), are remarkably identical (Fig. 5a and b). Both isotopes have to some extent similar variations to those of the monthly average air T values (Fig. 4b), with depleted isotopic ratios in the cold months from December to February and enriched ratios in the warmer or less wettest months (October and May). However, the monthly average δ^{18}O and δ^2H values, calculated on the basis of monthly data during the cold period (December to March), are clearly more depleted compared to those of the daily data, with the lowest isotopic ratios during the coldest month (January). Changes in the air T values in the atmosphere are generally the principal cause behind the seasonal variations of the stable isotope ratios in the Damascus rainfall. This trend of isotope variations strongly suggests that the depleted isotopic ratios usually occur when the monthly P-amount and RH values are both elevated.

The seasonal variation in the monthly average *d*-excess value is completely opposite to those of δ^{18}O and δ^2H values (Fig. 5c). The monthly average *d*-excess values calculated on the basis of monthly data are generally equal or slightly different from those of the daily data, especially during the cold period from December to March. However, the monthly average *d*-excess values, calculated on the basis of daily data during the warmer months (October, November, April and May), are clearly higher than those calculated for all monthly data. A good relationship is found between the seasonal variations in the monthly average *d*-excess and monthly average RH values, with high *d*-excess values (>14‰) during the wettest months (December to March), and lower monthly average *d*-excess values (<10‰) at the beginning and at the end of the rainy season. This evolution trend strongly reflects the influence of the enriched moisture (*d*≈30‰), produced from the MS (Gat et al., 2003), likely as a result of the strong interactions occurring between the enriched moisture existing over this sea with the humid air masses passing over the MS, specifically during the period from December to February. This isotopic exchange also explains the significant increase in the *d*-excess value in the rains falling all around the Mediterranean region (IAEA, 2005b).

The seasonal variations in the monthly average ^{3}H concentrations in the Damascus rainfall calculated on the basis of both daily and monthly data are marked by slight fluctuations around ≈3–6 TU during the period from October to February (Fig. 5d). Then, by the beginning of March, a gradual build-up in this parameter is
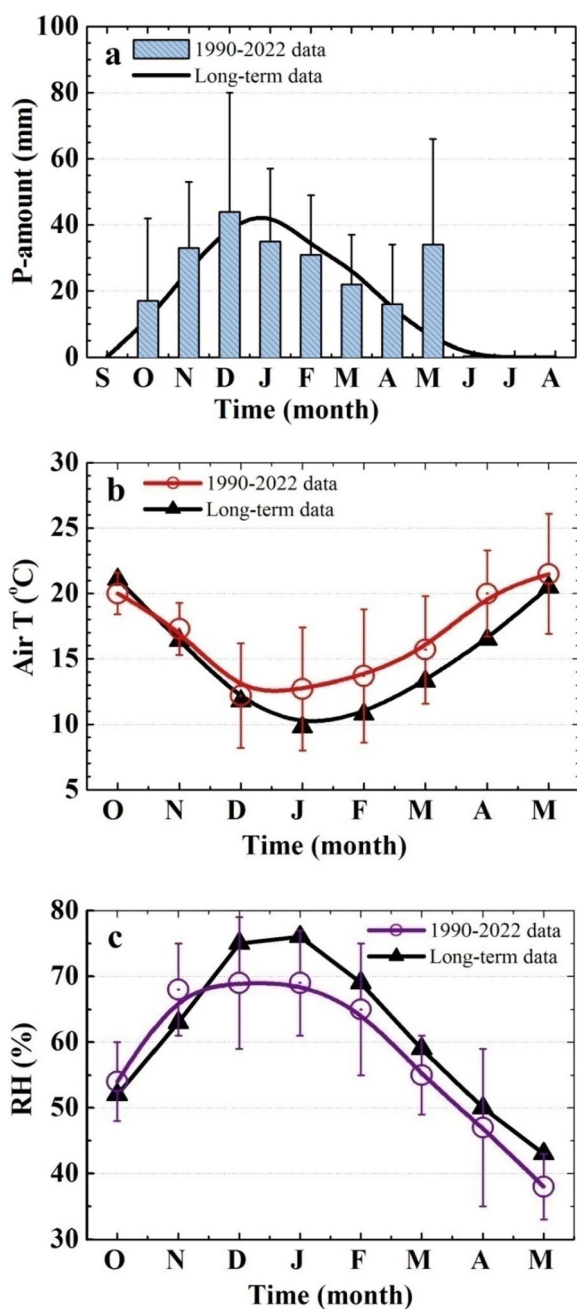
Fig. 4 Temporal variations in monthly averages and SD values for P-amount (**a**), air T (**b**) and RH (**c**) values during the rainy season

observed, up to values greater than 9 TU during April and May (monthly data) or 15 TU in April (daily data). This evolution clearly reflects the phenomenon so-called spring leak, which usually occurs during the spring season, likely as a result of the continuous injection of high ^3H loads from the troposphere to the ambient atmosphere (Rozanski et al., 1991; Ehhalt et al., 2002; Harms et al., 2016).

3.6 Annual variability of meteorological parameters

Distribution of the long-term annual P-amount values recorded at Mazzeh station, the closest station to the sampling site, during the period from 1919 to 2022 shows a range from ≈50 mm up to ≈350 mm, with an average value of ≈208±70 mm and a coefficient of variation of 34% (Fig. 6a). A dozen of water years ($P > 350$ mm) can be considered as wet ones, while only 8 years ($P < 100$ mm) can be classified as dry ones. Although the annual P-amount values recorded during 1919–1969 varied in a rather similar range (53–354 mm), and have an identical coefficient of variation (34%) compared to the period 1919–2022, the average P-amount value (≈213±72 mm), calculated for the period 1919–1969 is more elevated compared to the long-term average value (208 mm), calculated for the period 1919–2022. The distribution of P-amounts over a period of ≈1 century permits to observe a decrease of ≈−3.1 mm/decade (Table 4). However, when considering the distribution of this parameter at the sampling station during the period 1990–2019, a decreasing gradient of ≈−9 mm/decade is found (Fig. 6b). This variation trend could be considered as a representative evolution of the rainfall shortage associated with the climate change. The annual P-amount values during 1990–2022, which varied nearly in a similar range to those of the long-term data (86–337 mm), and have a similar coefficient of variation (34%), have an average of ≈185±67 mm. This means that the annual average P-amount during the last three decades has decreased by ≈23 mm, relative to the period 1919–1989 (Table 4), and by about ≈28 mm, relative to the period 1919–1969. This significant decrease in P strongly proves the effect of climate change, as previously also shown in the unusually high rain showers in October and May and low rain events in January and February (Fig. 4a).

In order to assess the drought stress on P time series, the index (SPI), as the standard deviations from the median (Sarker et al., 2021), or as the probability distribution function of P record during a long-term period of at least 30 years, was computed (Fig. 7). Accordingly, the variation in this index during the studied period shows a range from −2.2 (1960) to 2.1 (1953 and 1945). This means thus that the intensity of the drought stress (negative SPI values) has changed between normal (0 to −0.5) and severe (−1 to −2) classes (Hao & Singh, 2015). By adapting a polynomial curve of 4th order to fit with all SPI values during the period 1919–2022, it can be observed that the fitted curve over the period 1970–2022 is marked by a negative SPI trend, whereas it is positive over the previous period (Fig. 7). However, by plotting a second polynomial curve of the same order for the period 1990–2022, it was found that the correlation coefficient of the fitted last curve ($R^2 = 0.08$ and *p*-value < 0.0001) was
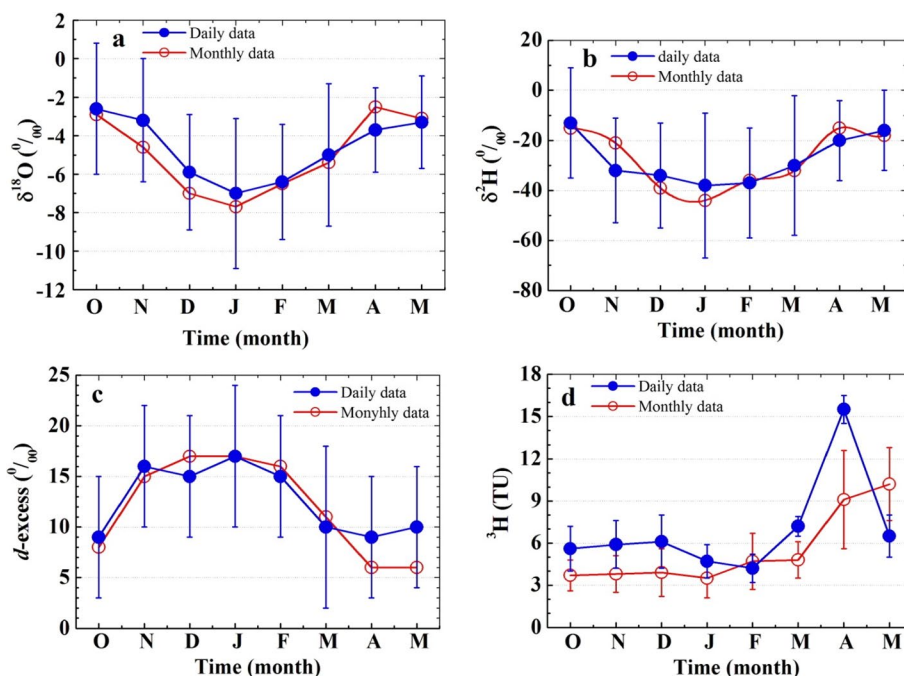
Fig. 5 Temporal variations in monthly averages and SD values for $\delta^{18}O$ (**a**), δ^2H (**b**), *d*-excess (**c**) and ^3H (**d**) values during the rainy season
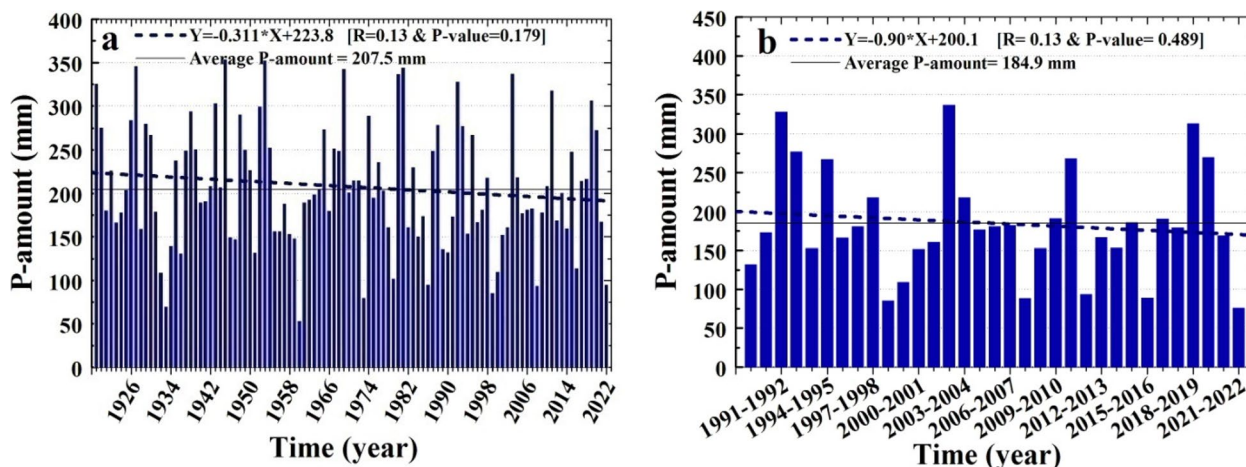

Fig. 6 Distribution of long-term annual P-amount values recorded at Mazzeh station during 1919–2022 (**a**) and at the sampling Soumaria station during 1990–2022 (**b**)

higher than the first one ($R^2 = 0.02$ and *p*-value < 0.0001), with also more severe drought stress (higher SPI values) during the period 1994–2012.

In all cases, the effect of climate change on the rain shortage in the Damascus region is shown by a decrease of ≈−13%, relative to the period 1919–1969. However, the decline estimated in this study in P-amounts is clearly still lower than the average value (17%), previously given by Abou Zakhem and Kattaa (2016), based on data covering the period 1941–2000. A significant reduction in

the annual P-amount values (5–30%) is expected during 2040–2099, relative to the period 1961–1990 (Lelieveld et al., 2012), and a similar decrease is also expected at a number of stations in the vicinity of the Figeh spring near Damascus during 2040–2069 (Smiatek et al., 2013).

The distribution of the long-term annual air T values recorded at Mazzeh station during 1919–2022 (Fig. 8a) shows a range from 15.2 °C up to 19.6 °C, with an average value of 17.0 ± 0.9 °C and a coefficient of variation of ≈5%. The temporal evolution of annual air T values

Table 4 Regression parameters of the linear relationships between annual P-amount, air T and RH values versus time and between annual $\delta^{18}O$, δ^2H, *d*-excess and ^3H values versus time for the rainfall collected at the Damascus-Soumaria station during the period 1990–2022

Relationship	Type of data	Time period	Slope	*Y*-intercept	R^2	N	*P*-value
P-time	Annual amount	1919–2022	-0.31 ± 0.23	223.8 ± 13.9	0.02	104	0.179
		1919–1989	-0.33 ± 0.24	224.6 ± 17.3	0.01	71	0.435
		1990–2022	-0.90 ± 1.28	200.1 ± 24.9	0.02	33	0.489
T-time	Annual average	1919–2022	0.019 ± 0.002	16.0 ± 0.1	0.40	104	< 0.0001
		1919–1989	0.001 ± 0.003	16.6 ± 0.1	0.00	71	0.831
		1990–2022	0.064 ± 0.01	16.8 ± 0.2	0.58	33	< 0.0001
RH-time	Annual average	1990–2022	-0.027 ± 0.08	49 ± 2.0	0.01	22	0.746
^{18}O-time	Annual average	1990–2022	0.050 ± 0.03	-6.65 ± 0.8	0.11	22	0.152
	Annual AWM		0.030 ± 0.03	-7.86 ± 0.6	0.07	22	0.257
^2H-time	Annual average	1990–2022	0.317 ± 0.21	-37.4 ± 5.0	0.10	22	0.156
	Annual AWM		0.112 ± 0.18	-43.3 ± 4.2	0.02	22	0.541
d-excess-time	Annual average	1990–2022	-0.091 ± 0.08	15.8 ± 1.8	0.07	22	0.260
	Annual AWM		-0.112 ± 0.07	19.4 ± 1.6	0.13	22	0.008
^3H-time	Annual average	1990–2022	-0.042 ± 0.04	6.3 ± 1.0	0.05	22	0.339
	Annual AWM		-0.040 ± 0.05	5.9 ± 1.0	0.04	22	0.379

during 1990–2019 is marked by variations from 15.9 to 19.6 °C, with an average value of 17.9 ± 0.8 °C and a coefficient of variation of ≈4% (Fig. 8b). The temporal evolution of annual air T values during 1919–1969 is marked by a slight continuous increase (≈+0.01 °C/decade), while it is clearly much higher (≈+0.64 °C/decade) during 1990–2022. The increasing gradient in the annual air T values during 1919–1969 fluctuated between 15.2 and 18.0 °C, with an average value of 16.6 ± 0.6 °C, and a coefficient of variation of ≈4%. This distribution strongly proves that the annual average air T value during the last three decades has increased by ≈+1.2 °C, compared to

Fig. 7 Distribution of long-term annual SPI values calculated for Mazzeh station data during 1919–2022 and plots of the fitted polynomial curves of the 4th order during the period 1919–2022 (blue line) and the period 1990–2022 (red line)

that recorded one century before. If this parameter continues increasing at the same gradients (Table 4), the annual air T value by the end of the twenty-first century is expected to attain ≈23 °C, i.e. higher by ≈5 °C, compared to the current air T values. Scenarios of climate change in the Mediterranean regions predicted an increase of ≈1.5–2.8 °C in the annual air T value in 2050 (Dai, 2011). The annual average air T value at Damascus during 2070–2099 was simulated to increase by +4.8 °C, relative to the period 1961–1990 (Smiatek et al., 2013).

The annual average RH values recorded at the sampling station during 1990–2022 varied within the range of 42–56%, with an average annual RH value of ≈49 ± 3% (Fig. 9). The temporal variation in this parameter generally reflects a small reduction (≈−0.3%/decade). If this parameter continues to decline at the same rate, the annual average RH value at the end of this century is expected to decrease by ≈2%, relative to the current RH values, meaning thus that this parameter is approximately the least affected by the consequences associated with climate change.
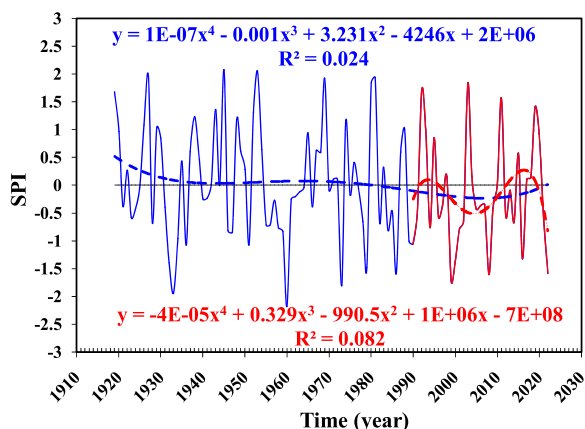
3.7 Annual variability of P isotopes

The regression parameters for the linear relationships established between the annual values in $\delta^{18}O$, δ^2H, *d*-excess and ^3H versus time, relative to the RW samples collected at the sampling station during 1990–2022, are shown in Table 4. Accordingly, the points representing the annual values in $\delta^{18}O$ and δ^2H, calculated as arithmetic averages, are clearly higher than those calculated as AWM values. The temporal variations in both stable

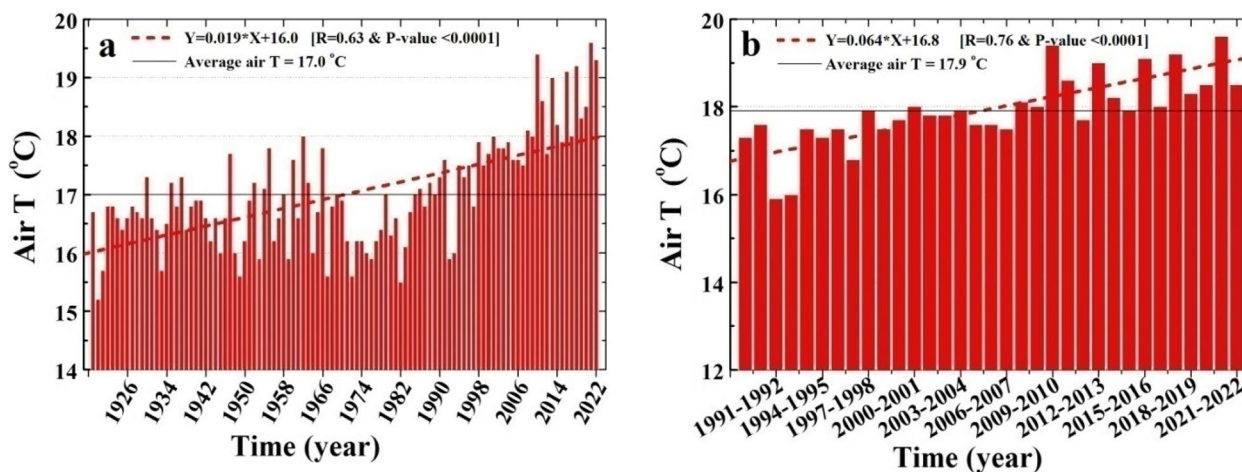**Fig. 8** Distribution of long-term annual average air T values recorded at Mazzeh station during 1919–2022 (**a**) and at the sampling Soumaria station during 1990–2022 (**b**)
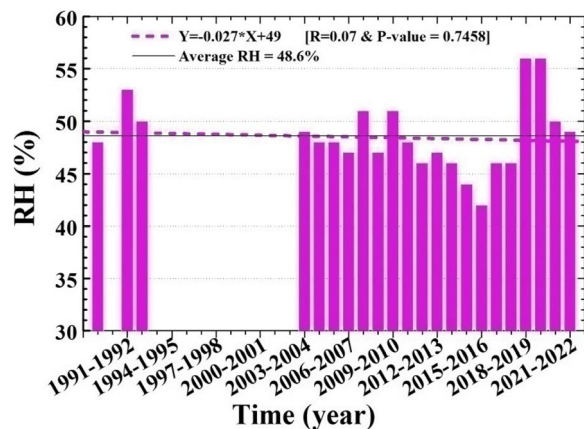

Fig. 9 Temporal variation in annual average RH values recorded at the sampling Soumaria station during 1990–2022

isotopes over time show generally a detectable isotopic increase in the RW composition with increasing time (Fig. 10a and b). The average increasing gradients are $\approx +0.3$–0.5‰ and $\approx +1.1$–3.2‰ per decade for $\delta^{18}O$ and $\delta^{2}H$, respectively. This means that the annual $\delta^{18}O$ and $\delta^{2}H$ values in the RW samples at the beginning of 2050 will be increased by $\approx +1.0$–1.5‰ (≈ 15–20%) and $\approx +3$–10‰ (≈ 10–25%) for $\delta^{18}O$ and $\delta^{2}H$, respectively, compared to the current annual $\delta^{18}O$ and $\delta^{2}H$ ratios.

The temporal variations in the annual d-excess values and annual ^{3}H concentrations show oppositely a significant decrease with increasing time (Fig. 10c and d). Although the annual AWM d-excess values are slightly higher than the annual average d-excess values, the temporal variations in the d-excess values in both cases are rather similar. The annual average d-excess values vary in the range of 7–22‰ whereas fluctuate from 11 to 23‰

in the case of annual AWM d-excess values. The correlation coefficient calculated for the relationship between annual AWM d-excess values versus time is relatively high ($R = 0.35$) compared to remaining isotopic parameters (Table 4). This relationship indicates a decrease of ≈ -1.1‰ per decade in the AWM d-excess value, while a reduction of ≈ -0.9‰ is found in the case of the annual average d-excess values. This decrease clearly means that after three decades, the d-excess values will be lower by ≈ -2.7–3.3‰, compared to the current d-excess values. This decline also means that the predicted d-excess values during 2050 will be around 11–13‰, which are much lower than the value 22‰, given by Nir (1967) for this region, approaching the value 10‰, given as an average for the Globe (Craig, 1961).

The annual average concentrations of ^{3}H in the RW samples in the Damascus area during the study period varied from 8.5–8.7 TU (1989–1990) to 2.3–2.5 TU (2012–2013), with an average value of $\approx 4.8 \pm 2.6$ TU. The gradients of ^{3}H degradation over time (-0.40 and -0.42 TU/decade for annual AWM and annual average ^{3}H values, respectively) are rather similar (Fig. 10d). However, the annual ^{3}H values calculated for the year 2018 was relatively high (> 7 TU), likely because of the heavy rains occurred in May 2018, likely because of the "spring leak" effect, usually associated with injection of high ^{3}H loads and bilateral exchange among the stratosphere, troposphere and ambient atmosphere (Ehhalt et al., 2002; Harms et al., 2016). Due to this effect, the concentration of ^{3}H in April 1990 was also elevated (13.6 TU), compared to the value (4.3 TU) measured in December 1989 (Kattan, 1997b). The annual variability in this radioisotope during the last three decades shows a progressive decline towards low ^{3}H levels (< 5 TU), which is identical
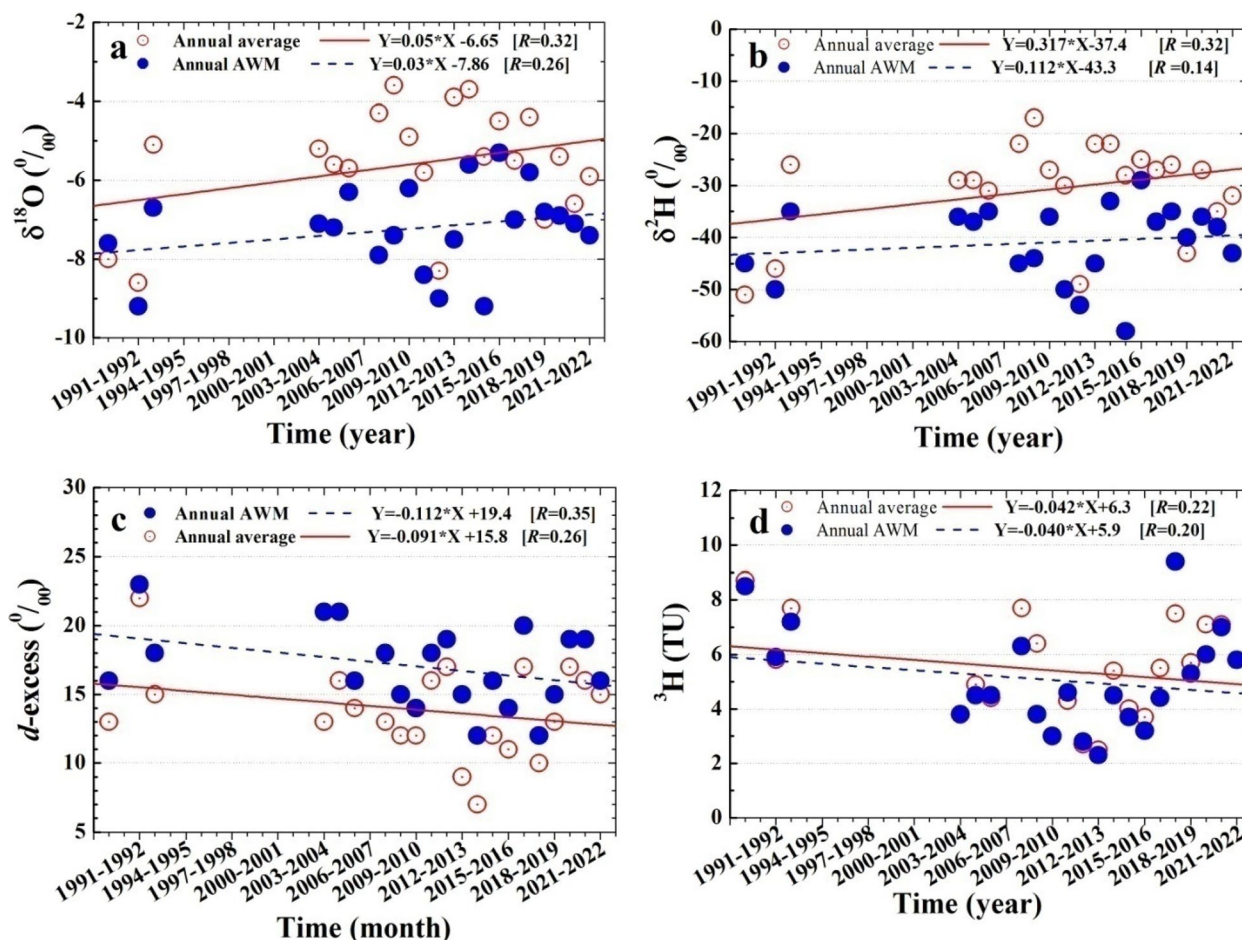
Fig. 10 Temporal variations in annual $\delta^{18}O$ (**a**), δ^2H (**b**), *d*-excess (**c**) and ^3H (**d**) values measured in the RW samples collected at the Soumaria station during 1990–2022

to those observed before the start of the nuclear weapons tests (Eriksson, 1983). Hence, as the nuclear weapon experiments had ceased completely since the 1980s, the previous ^3H loads due to anthropogenic sources are currently considered to be of minimal levels, likely because of ^3H decay. The decline of ^3H concentration in the current P towards low levels strongly suggests that this radioactive isotope is primarily produced by the natural cosmogenic reactions in the upper atmosphere.

3.8 Comparison between the annual time-series variability of studied parameters

To identify the similarities and compare between the time-series variability of the different meteorological parameters and assess their possible controls on the isotopic data, the paired *t*-test analysis was carried out by adapting the null hypothesis, i.e. no variation exists between variables, or that a single variable is no different than zero (Bevans, 2022). The *t*-values, calculated based on the multivariate analysis between the different

parameters of the entire dataset (Table 5), show that the true difference in means is different from 0, and that most of the *p*-values are < 0.0001. In all cases, the *p*-values are much smaller than 0.03. Only a small number of *p*-values are between 0.03 and 0.07. The *t*-values calculated for all variables with respect to time range from 2.4 to 25.2, with negative values in the case of P and RH parameters, as both variables tend to decrease with increasing time. The results also prove that the variability trends in the stable isotopes with time are rather similar ($15 < t$-value < 25) but distinctly different from those of air T and *d*-excess (t-value < 5). Also, it can be observed that the variability trends in P and RH are of the same order ($-13.3 < t$-value < -12.6). When considering the variability of all parameters against P, it is found that the *t*-values are almost of the same order, with slight significant differences in the *t*-value between 8.7 (RH) and 13.6 (annual AWM ^2H). When comparing the variability trends of all parameters with respect to air T parameter, more significant differences are found in the *t*-value, changing

Table 5 Matrix of *t*-values calculated based on the multivariate analysis between the different parameters of the rainfall collected at the Damascus-Soumaria station during the period 1990–2022

Variable	Time	P	T	RH	Annual average ^{18}O	Annual AWM ^{18}O	Annual average ^{2}H	Annual AWM ^{2}H	Annual average *d*-excess	Annual AWM *d*-excess
P	−13.3	0								
T	2.4	10.4	0							
RH	−12.6	8.7	−35.1	0						
Annual average ^{18}O	15.1	11.8	81.2	57.4	0					
Annual AWM ^{18}O	16.1	11.9	93.7	62.2	4.7	0				
Annual average ^{2}H	20.9	12.9	27.0	36.1	15.8	13.2	0			
Annual AWM^{2}H	25.2	13.6	33.9	44.5	20.4	21.6	4.5	0		
Annual average *d*-excess	3.8	10.9	4.8	44.2	−19.0	−23.2	−18.3	−26.2	0	
Annual AWM *d*-excess	2.5	10.7	2.0	41.6	−25.0	−25.4	−21.6	−25.6	−4.1	0
Annual AWM ^{3}H	9.0	11.4	28.8	52.6	−21.4	−29.0	−18.5	−26.2	11.4	14.8

The degree of freedom (*DF*) is equal to 19 for all variables, except P, for which DF is equal to 31. All *p*-values are < 0.0001, except the following paired parameters: T-time (*p*-value < 0.0256), annual average *d*-excess-time (*p*-value = 0.0013), annual AWM *d*-excess-time (*p*-value = 0.0213), annual AWM *d*-excess-T (*p*-value = 0.0652) and annual average *d*-excess-annual AWM *d*-excess (*p*-value = 0.0007)

between 2.0 (annual AWM *d*-excess) and 93.7 (annual AWM ^{18}O), meaning thus that the role of air T variability is accompanied by different effects on the isotopic variables. When comparing the similarities of the different variables with respect to RH parameter, it is found that the *t*-values are fluctuating between 36.1 (annual average ^{2}H) and 62.2 (annual AWM ^{18}O), meaning thus that the RH parameter has a moderate influence on most isotopes.

3.9 Meteorological controls on variability of P stable isotopes

Changes in the ambient weather conditions, specifically air T, P-amount and RH values, are usually the principle causes for the temporal and spatial variations of the isotopic composition of meteoric water (Dansgaard, 1964; Kumar et al., 2010; Terzer et al., 2013). However, these factors are not always the only causes for the variability of such isotopes, as other factors such as the isotopic composition of the water vapour in the atmosphere, the origins and trajectories of humid air masses may contribute altogether in the formulation of the isotopic signature of rainfall (Lawrence et al., 1982; Liotta et al., 2008; Liu et al., 2011; Jeelani et al., 2018; Vystavna et al., 2021).

The regression parameters for the linear relationships, calculated between the annual average and annual AWM values of δ^{18}O, δ^{2}H and *d*-excess versus the annual average values of P-amount, air T and RH values recorded for the Damascus rainfall during 1990–2022 (Table 6), show that the correlation coefficients (R^2) calculated on the basis of annual average values are mostly higher or equal to those of the annual AWM values. Although the R^2 values for the relationships δ^{18}O-T, δ^{2}H-T and *d*-excess-T

are moderate ($0.07 < R^2 < 0.29$), they are much higher than those of the other meteorological parameters, meaning thus that the effect of air T is the primary controlling factor affecting the annual variability of P stable isotopes. The difference in the R^2 value between the two methods is mostly below 3%.

The effect of P-amount on the annual variability of P stable isotopes is shown by small isotopic degradations (≈ 0.4–0.6‰ and 1.5–3.3‰ for δ^{18}O and δ^{2}H, respectively) and weak correlations ($0.02 < R^2 < 0.16$), with the increasing of annual P-amount value by 100 mm (Fig. 11a and b). However, this effect is relatively better in the case of variations in the annual *d*-excess values ($R^2 = 0.16$) and reflected by an increase of ≈ 1.7‰ (AWM data) and ≈ 1.8‰ (average data), with the increasing of annual P-amount value by 100 mm (Fig. 11c). Previous estimates of this effect on the monthly variations of P stable isotopes during 1989–2006 showed a decrease of $\approx -0.7 \pm 0.3$‰ and $\approx -2.9 \pm 2.1$‰ for δ^{18}O and δ^{2}H, respectively, accompanied with an increase of $+2.7 \pm 0.6$‰ in the *d*-excess value, with the increasing of monthly P-amount value by 10 mm (Kattan, 2019).

The T effect on the annual variability of δ^{18}O and δ^{2}H values is reflected by enrichments of ≈ 0.50–0.58‰/°C and $\approx +2.2$–2.7‰/°C, respectively, with the increasing of annual air T value by 1 °C (Fig. 12a and b). The R^2 values in the case of the relationship δ^{18}O-T ($0.16 < R^2 < 0.17$) are generally higher than those calculated for the relationship δ^{2}H-T ($0.07 < R^2 < 0.10$). However, the strongest correlations are found for the relationship *d*-excess-T ($0.28 < R^2 < 0.29$). This relationship reflects a decrease of ≈ 1.8–1.9‰/°C in the annual *d*-excess value with the increasing of annual air T value by 1 °C (Fig. 12c).

Table 6 Regression parameters of the linear relationships between annual δ^{18}O, δ^2H and *d*-excess values versus annul P-amount, annual air T and annual RH values for the rainfall collected at the Damascus-Soumaria station during the period 1990–2022

Relationship	Type of data	Slope	*Y*-intercept	R^2	N	*p*-value
^{18}O-P	Annual average	-0.006 ± 0.004	-4.3 ± 0.8	0.12	22	0.136
	Annual AWM	-0.004 ± 0.004	-6.1 ± 0.8	0.06	22	0.305
^{2}H-P	Annual average	-0.033 ± 0.03	-23.4 ± 5.1	0.09	22	0.207
	Annual AWM	-0.015 ± 0.02	-35.5 ± 4.9	0.02	22	0.547
d-excess-P	Annual average	0.018 ± 0.01	10.4 ± 2.0	0.16	22	0.086
	Annual AWM	0.017 ± 0.01	13.3 ± 1.9	0.16	22	0.083
^{18}O-T	Annual average	0.58 ± 0.3	-16.0 ± 5.5	0.17	22	0.073
	Annual AWM	0.50 ± 0.3	-16.0 ± 4.9	0.16	22	0.079
^{2}H-T	Annual average	2.65 ± 1.9	-77.7 ± 34.7	0.10	22	0.182
	Annual AWM	2.15 ± 1.8	-77.3 ± 32.9	0.07	22	0.252
d-excess-T	Annual average	-1.88 ± 0.7	48 ± 13	0.28	22	0.016
	Annual AWM	-1.78 ± 0.7	49 ± 12	0.29	22	0.014
^{18}O-RH	Annual average	-0.13 ± 0.08	1.1 ± 4.1	0.12	22	0.130
	Annual AWM	-0.08 ± 0.08	-3.0 ± 3.8	0.05	22	0.325
^{2}H-RH	Annual average	-0.59 ± 0.5	-0.78 ± 26	0.07	22	0.273
	Annual AWM	-0.21 ± 0.5	-28 ± 25	0.01	22	0.681
d-excess-RH	Annual average	0.47 ± 0.2	-8.8 ± 9.6	0.24	22	0.030
	Annual AWM	0.42 ± 0.2	-4.0 ± 9.0	0.22	22	0.035

The enrichments in the annual δ^{18}O and annual δ^2H values are slightly higher than the monthly enrichment gradients ($\approx 0.5 \pm 0.12$‰/°C and $\approx 2.7 \pm 0.9$‰/°C for δ^{18}O and δ^2H, respectively), previously given for the Damascus rainfall during 1989–2006, with the increasing of monthly air T value by 1 °C (Kattan, 2019). The average decrease in the monthly *d*-excess value in the case of the aforementioned rainfall was $\approx 1.3 \pm 0.3$‰/°C, with the increasing of monthly air T value by 1 °C. In all cases, the enrichments in δ^{18}O value calculated for the Damascus rainfall are generally in a good accordance with the published δ^{18}O/ΔT gradients (>0.4‰/°C), given for rainfall in the Mediterranean countries (IAEA, 2005b). However, the monthly enrichments in δ^{18}O value are relatively much higher compared to the average monthly enrichment (0.4 ± 0.02‰/°C), given for the GNIP data (Rozanski et al., 1993).

The effect of RH has also a decisive influence on the variations of P stable isotopes (Gat, 1996). Changes in this parameter can principally affect the isotopic fractionation occurring either under equilibrium or kinetic conditions (Majoube, 1971). This effect is usually reflected by enrichments in heavy stable isotopes due to evaporation, as the lower the RH value, the higher the isotopic fractionation and the higher the evaporation (Clark & Fritz, 1997). The RH effect on the annual variations of P stable isotopes is marked by small depletions (≈ 0.8–1.3‰ and ≈ 2–6‰ for δ^{18}O and δ^2H, respectively), accompanied by an increase of ≈ 4–5‰ in the annual *d*-excess value,

with the increasing of annual RH value by 10% (Fig. 13). Previous estimates of this effect on the monthly P stable isotopes in the Damascus rainfall during 1989–2006 showed depletions of $\approx 2.2 \pm 0.5$‰ and $\approx 12.6 \pm 3.6$‰ for δ^{18}O and δ^2H, respectively, accompanied by an increase of $\approx 5.3 \pm 1.2$‰ in the monthly *d*-excess values, with the increasing of monthly RH value by 10% (Kattan, 2019).

4 Conclusions

Analysis of 22-year records of δ^{18}O and δ^2H, *d*-excess and ^{3}H values in the RW samples at the Damascus area during 1990–2022 and long-term time series of air T- and P-amount values during 1919–2022 is discussed. Daily and monthly composite RW samples are conjunctly used to characterize the seasonal and annual variability patterns of P isotopes at the Damascus station. The meteorological controls on the temporal variations of P isotopes are also quantified during the last three decades to assess the vulnerability to climate change in this region. The major conclusions that can be extracted from this study are the following:

- The seasonal variations in the monthly average δ^{18}O and δ^2H values, calculated on the basis of both daily and monthly data, are remarkably similar, with depleted isotopic ratios in the coldest months (December to February), specifically when P-amount and RH values are both elevated. However, the enriched isotopic ratios distinctly occur in the
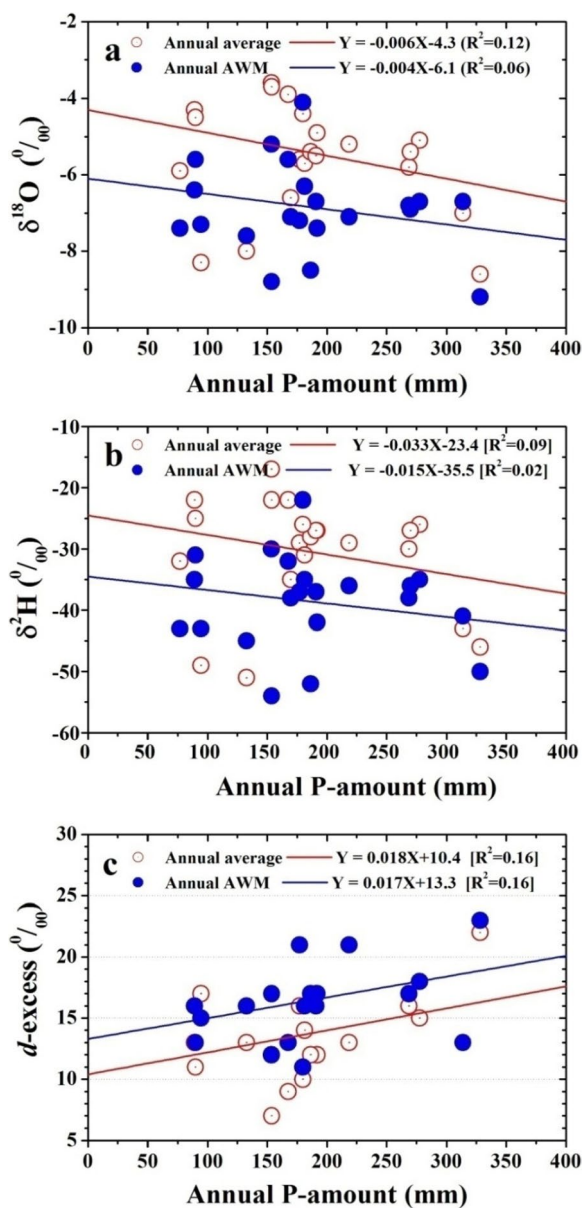
Fig. 11 Relationships between annual $\delta^{18}O$ and annual P-amount values (**a**), annual δ^2H and annual P-amount values (**b**) and annual *d*-excess and annual P-amount values (**c**) recorded at the Soumaria station during 1990–2022
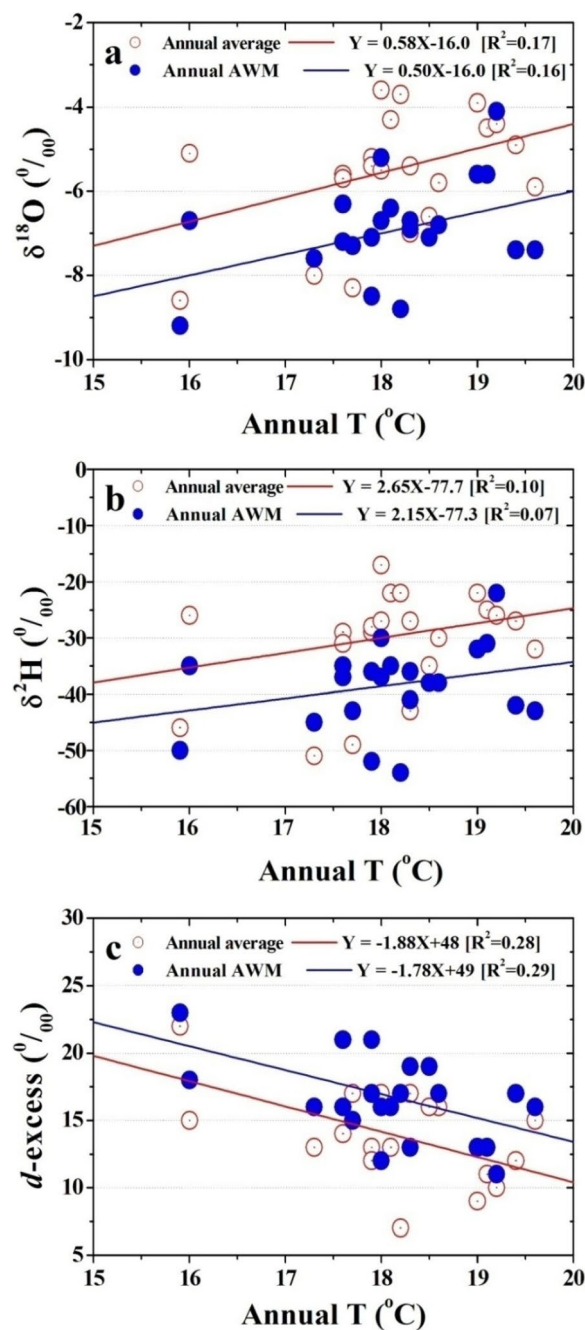

Fig. 12 Relationships between annual $\delta^{18}O$ and annual air T values (**a**), annual δ^2H and annual air T values (**b**) and annual *d*-excess and annual air T values (**c**) recorded at the Soumaria station during 1990–2022

warmer and less wettest months (October and May) and strongly prove that the change in air T value is the principal cause for the variability of P stable isotopes. The high ^3H concentrations (>9 TU), markedly measured in April and May, clearly reflect the "spring leak" phenomena, typically distinguished by injection of high ^3H loads, associated with bilateral exchange among the stratosphere, troposphere and atmosphere.

- The seasonal variation in the monthly average *d*-excess values is completely opposite to those of $\delta^{18}O$ and δ^2H values, with high *d*-excess values (*d* > 14‰) during the wettest months, when P-amount and RH values are both high, and lower values (*d* < 10‰) at the beginning and the end of the
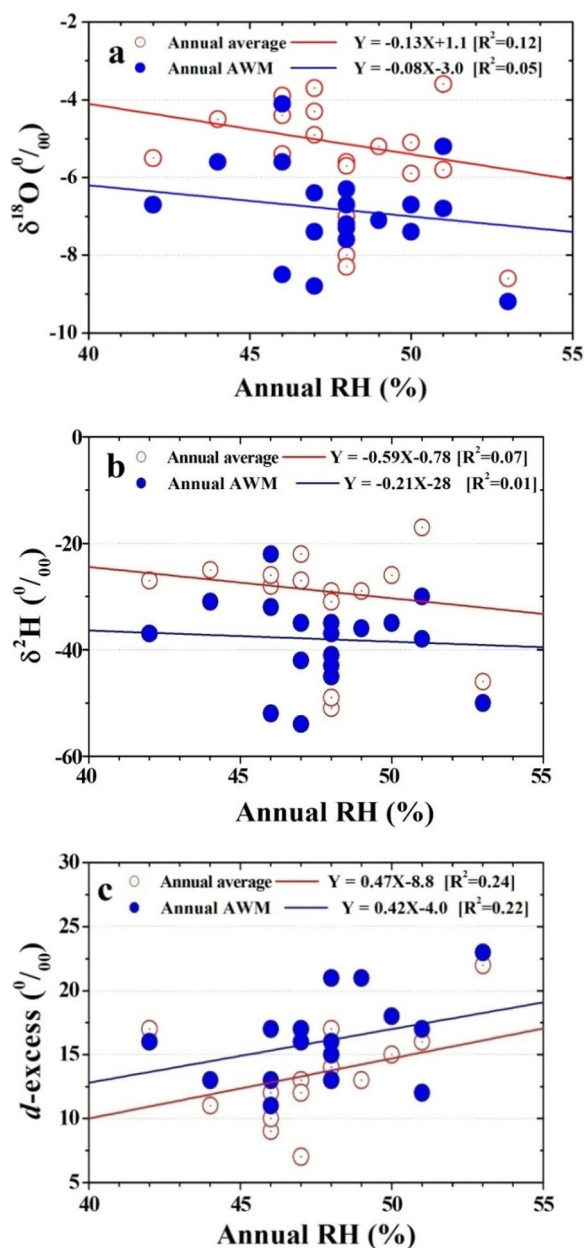
Fig. 13 Relationships between annual δ^{18}O and annual RH values (**a**), annual δ^2H and annual RH values (**b**) and annual *d*-excess and annual RH values (**c**) recorded at the Soumaria station during 1990–2022

rainy season. The good relationship between RH and *d*-excess values proves the efficacy of using the *d*-excess parameter as a marker for assessing secondary evaporation. The seasonal variation in the *d*-excess values strongly reflects the effect of interactions occurring between the humid air masses passing over the MS in winter and the enriched moisture ($d \approx 30‰$), produced by evaporation from this sea.

- The long-term annual variation of P-amount values recorded at the Damascus area during 1919–2022 clearly shows that the average P-amount value during the last three decades (185 ± 67 mm) is lower by ≈ 28 mm compared to the value (213 ± 72 mm), recorded during 1919–1969. The effect of climate change on rain shortage at the Damascus area is marked by a decrease of ≈ 11–13%, relative to the period 1919–1969, which is clearly lower than the rate (17%), given for the period 1941–2000.

- The distribution of the long-term annual air T values recorded at the Damascus area during 1919–2022 is marked by an increase gradient of $\approx +0.2$ °C/decade, which is remarkably much lower than the gradient ($+0.64$ °C/decade), determined for the period 1990–2022. This temporal evolution clearly reflects the impact of climate change affecting this region since the 1970s. The annual variation in the RH values during the period 1990–2022, which shows a small reduction gradient ($\approx -0.3\%$/decade), reveals that this parameter is the less affected by the consequences related to climate change.

- The linear relationships between annual average δ^{18}O and δ^2H values versus time indicate an increase of ≈ 0.3–0.5‰ and ≈ 1.1–3.2‰ per decade for δ^{18}O and δ^2H, respectively, associated by a decrease of ≈ 0.9–1.1‰/decade in the *d*-excess value.

- Variability of the annual average ^{3}H concentrations during the last three decades towards low levels (< 5 TU) strongly suggests the return back towards the cosmogenic production levels of ^{3}H in the upper atmosphere before the start of the nuclear experiment tests.

- The principal factor that strongly controls the seasonal and annual variability of P stable isotopes is the change in air T over time. This factor is reflected by significant isotopic enrichments (0.5–0.6‰ and 2.2–2.7‰ for δ^{18}O and δ^2H values, respectively) with the increase of annual air T value by 1 °C. The impacts of P-amount and RH are of minor importance. However, further causes, such as the secondary evaporation and enriched moisture produced from the MS, can conjunctly affect the variability of P isotopes in this semi-arid area.

- As P is an important component of the water cycle and the overall regional water availability is highly dependent on the cold P, which has continuously influenced by climate change, the findings gained from this study will certainly help to better improve the knowledge on the temporal variability patterns of P isotopes and properly use these natural tracers in assessing the risks due to climate change on the quality and quantity of renewable surface and groundwater resources in the Eastern Mediterranean region.

Authors' contributions

This article was entirely written by Zuhair Kattan, who carried out the interpretation and discussion of the isotopic results related to this paper. Saeid Nasser collected most of the rainfall samples and relavent meteorological data. Both authors read and approved the final manuscript.

Declarations

Competing interests

The authors declare that they have no competing interests.

References

Abou Zakhem, B., & Hafez, R. (2007). *Chemical and isotopic composition of precipitations in Syria. AECS-G\RSS No. 729.* Atomic Energy Commission of Syria.

Abou Zakhem, B., & Kattaa, B. (2016). Investigation of hydrological drought using cumulative standardized precipitation index (SPI 30) in the Eastern Mediterranean region (Damascus, Syria). *Journal of Earth System Science*, *125*(5), 969–984. https://doi.org/10.1007/s12040-016-0703-0.

Aggarwal, P. K., Frohlich, K., Kulkarni, K. M., & Gourcy, L. L. (2004). Stable isotope evidence for moisture sources in the Asian summer monsoon under present and past climate regimes. *Geophysical Research Letters*, *31*, L08203. https://doi.org/10.1029/2004GL019911.

Aggarwal, P. K., Alduchov, O. A., Froehlich, K. O., Araguas-Araguas, L. J., Sturchio, N. C., & Kurita, N. (2012). Stable isotopes in global precipitation: A unified interpretation based on atmospheric moisture residence time. *Geophysical Research Letters*, *39*(11), L11705. https://doi.org/10.1029/2012GL051937.

Aizen, V. B., Aizen, E. M., Fujita, K., Nikitin, S., Kreutz, K., & Takeuchi, N. (2005). Stable-isotope time series and precipitation origin from firn cores and snow samples, Altai glaciers, Siberia. *Journal of Glaciology*, *51*(175), 637–654.

Akata, N., Kakiuchi, H., Shima, N., Iyogi, T., Momoshima, N., & Hisamatsu, S. I. (2011). Tritium concentrations in the atmospheric environment at Rokkasho, Japan before the final testing of the spent nuclear fuel reprocessing plant. *Journal of Environmental Radioactivity*, *102*(9), 837–842.

Akers, P. D., Welker, J. M., & Brook, G. A. (2017). Reassessing the role of temperature in precipitation oxygen isotopes across the eastern and central United States through weekly precipitation-day data. *Water Resource Research*, *53*, 7644–7661.

Allen, S. T., Jasechko, S., Berghuijs, W. R., Welker, J. M., Goldsmith, G. R., & Kirchner, J. W. (2019). Global sinusoidal seasonality in precipitation isotopes. *Hydrological Earth System Science*, *23*(8), 3423–3436. https://doi.org/10.5194/hess-23-3423-2019.

Angelidis, P., Maris, F., Kotsovinos, N., & Hrissanthou, V. (2012). Computation of drought index SPI with alternative distribution functions. *Water Resources Management*, *26*, 2453–2473. https://doi.org/10.1007/s11269-012-0026-0.

Angert, A., Lee, J. E., & Yakir, D. (2008). Seasonal variations in the isotopic composition of near surface water vapor in the eastern-Mediterranean. *Tellus*, *B60*, 674–684. https://doi.org/10.1111/j.1600-0889.2008.00357.x.

Bajjali, W. (2012). Spatial variability of environmental isotope and chemical content of precipitation in Jordan and evidence of slight change in climate. *Applied Water Science*, *2*, 271–283. https://doi.org/10.1007/s13201-012-0046-1.

Bevans, R. (2022). *An introduction to t tests: Definitions, formula and examples.* Scribbr. https://www.scribbr.com/statistics/t-test/.

Bhat, N. A., & Jeelani, G. (2015). Delineation of the recharge areas and distinguishing the sources of karst springs in Bringi watershed, Kashmir Himalayas using hydrochemistry and environmental isotopes. *Journal of Earth System Science*, *124*, 1667–1676. https://doi.org/10.1007/s12040-015-0629-y.

Bowen, G. J., & Revenaugh, J. (2003). Interpolating the isotopic composition of modern meteoric precipitation. *Water Resource Research*, *39*(10), 1299. https://doi.org/10.1029/2003WR002086.

Clark, I., & Fritz, P. (1997). *Environmental isotopes in hydrogeology*. Lewis Publishers.

Coplen, T. B. (1996). New guidelines for reporting stable hydrogen, carbon, and oxygen isotope-ratio data. *Geochimica Et Cosmochimica Acta*, *60*, 3359–3360.

Craig, H. (1961). Isotope variations in meteoric waters. *Science*, *133*, 1702–1703.

Criss, R. E. (1999). *Principles of stable isotope distribution*. Oxford University Press.

Cruz, F. W., Burns, S. J., Karmann, I., Sharp, W. D., Vuille, M., Cardoso, A. O., Ferrari, J. A., Silva Dias, P. L., & Viana, O. (2005). Insolation-driven changes in atmospheric circulation over the past 116,000 years in subtropical Brazil. *Nature*, *434*, 63–66.

Dai, A. (2011). Drought under global warming: A review. *Wiley Interdisciplinary Reviews: Climate Change*, *2*(1), 45–65. https://doi.org/10.1002/wcc.81.

Dansgaard, W. (1964). Stable isotopes in precipitation. *Tellus*, *16*, 436–468.

Davis, S. M., Hegglin, M. I., Fujiwara, M., et al. (2017). Assessment of upper tropospheric and stratospheric water vapor and ozone in reanalyses as part of S-RIP. *Atmospheric Chemistry and Physics Journal*, *17*, 12743–12778. https://doi.org/10.5194/acp-17-12743-2017.

Ehhalt, D. H., Rohrer, F., Schauffler, S., & Pollock, W. (2002). Tritiated water vapor in the stratosphere: Vertical profiles and residence time. *Journal of Geophysical Research*, *107*(D24), 4757.

Eriksson, E. (1983). Stable isotopes and tritium in precipitation. *Guidebook on nuclear techniques in hydrology, Technical Report Series No 91* (pp. 19–33). IAEA.

Gat, J. R. (1996). Oxygen and hydrogen isotopes in the hydrologic cycle. *Annual Review of Earth and Planetary Sciences*, *24*, 225–262.

Gat, J. R., & Carmi, I. (1970). Evolution of the isotopic composition of atmospheric waters in the Mediterranean Sea area. *Journal of Geophysical Research*, *75*, 3039–3048.

Gat, J. R., Klein, B., Kushnir, Y., Roether, W., Wernli, H., Yam, R., & Shemesh, A. (2003). Isotope composition of air moisture over the Mediterranean Sea: An index of the air-sea interaction pattern. *Tellus*, *B55*(5), 953–965. https://doi.org/10.1034/j.1600-0889.2003.00081.x.

Giorgi, G., & Lionello, P. (2008). Climate change projections for the Mediterranean region. *Jjournal Global and Planetary Change*, *63*, 90–104.

Gonfiantini, R. (1978). Standard for stable isotope measurements in natural compounds. *Nature (London)*, *271*, 534–536.

Gonfiantini, R., Roche, M. A., Olivry, J. C., Fontes, JCh., & Zuppi, G. M. (2001). The altitude effect on the isotopic composition of tropical rains. *Chemical Geology*, *181*, 147–167. https://doi.org/10.1016/S0009-2541(01)00279-0.

Guiot, J., & Cramer, W. (2016). Climate change: The 2015 Paris Agreement Thresholds and Mediterranean basin ecosystems. *Science*, *354*, 465–468. https://doi.org/10.1126/science.aah5015.

Hao, Z., & Singh, V. P. (2015). Drought characterization from a multivariate perspective: A review. *Journal of Hydrology*, *527*, 668–678.

Harms, P. A., Visser, A., Moran, J. E., & Esser, B. K. (2016). Distribution of tritium in precipitation and surface water in California. *Journal of Hydrology*, *534*, 63–72.

Hendricks, M. B., DePaolo, D. J., & Cohen, R. C. (2000). Space and time variation of $\delta^{18}O$ and δD in precipitation; can paleotemperature be estimated from ice cores? *Global Biogeochemtry Cycles*, *14*, 851–861.

Hoefs, J. (2009). *Stable isotope geochemistry* (6th ed.). Springer-Verlag.

IAEA, International Atomic Energy Agency. (2005a). Isotopes in the water cycle. In P. K. Aggarwal, J. R. Gat, & K. F. O. Froehlich (Eds.), *Past, present and future of a developing science*. Springer.

IAEA, International Atomic Energy Agency. (2005b). *Isotopic composition of precipitation in the Mediterranean Basin in relation to air circulation patterns and climate. TECDOC-1453.* IAEA.

IAEA-WMO, International Atomic Energy Agency-World Meteorological Organization. (2021). *Global network of isotopes in precipitation, the GNIP database*. IAEA. https://www.iaea.org/water.isohis.iaea.org.

Jeelani, G., Deshpande, R. D., Galkowski, M., & Rozanski, K. (2018). Isotopic composition of daily precipitation along the southern foothills of the Himalayas: Impact of marine and continental sources of atmospheric moisture. *Atmospheric Chemistry and Physics*, *18*, 8789–8805. https://doi.org/10.5194/acp-18-8789-2018.

Johnsen, S., Dansgaard, W., & White, J. (1989). The origin of Arctic precipitation under present and glacial conditions. *Tellus*, *B41*, 452–468.

Karim, A., & Veizer, J. (2002). Water balance of the Indus River basin and moisture source in the Karakoram and Western Himalayas: Implications from hydrogen and oxygen isotopes in river water. *Journal of Geophysical Research-Atmosphere*, *107*, 4362. https://doi.org/10.1029/2000JD000253.

Kattan, Z. (1997a). Environmental isotope study of the major karst springs in Damascus limestone aquifer systems: Case of the Figeh and Barada springs. *Journal of Hydrology*, *193*, 161–182.

Kattan, Z. (1997b). Chemical and environmental isotope study of precipitation in Syria. *Journal of Arid Environments*, *35*, 601–615.

Kattan, Z. (2019). Factors controlling stable isotopes variability in precipitation in Syria: Statistical analysis approach. *Journal of Earth System Science*, *128*, 1–25. https://doi.org/10.1007/s12040-019-1142-5.

Kattan, Z. (2021). Spatial mapping of atmospheric precipitation isotopes in Syria. *Asian Journal of Atmospheric Environment*, *15*(2), 2021009. https://doi.org/10.5572/ajae.2021.009.

Kelley, C. P., Mohtadi, S., Cane, M. A., Seager, R., & Kushnir, Y. (2015). Climate change in the Fertile Crescent and implications of the recent Syrian drought. *Proceedings of the National Academy of Sciences, USA*, *112*(11), 3241–3246. https://doi.org/10.1073/pnas.1421533112.

Kendall, C., & Coplen, T. B. (2001). Distribution of oxygen-18 and deuterium in river waters across the United States. *Hydrological Processes*, *15*, 1363–1393.

Klein, E. S., Nolan, M., McConnell, J., Sigl, M., Cherry, J., Young, J., et al. (2016). McCall Glacier record of Arctic climate change: Interpreting a northern Alaska ice core with regional water isotopes. *Quaternary Science Reviews*, *131*, 274–284.

Kumar, U. S., Kumar, B., Rai, S. P., & Sharma, S. (2010). Stable isotope ratios in precipitation and their relationship with meteorological conditions in the Kumaon Himalayas, India. *Journal of Hydrology*, *391*, 1–8.

Lawrence, J. R., Gedzelman, S. D., White, J. W. C., Smiley, D., & Lazov, P. (1982). Storm trajectories in eastern US, D/H isotopic composition of precipitation. *Nature*, *296*(5858), 638–640.

Lee, J. E., & Fung, I. (2008). "Amount effect" of water isotopes and quantitative analysis of post-condensation processes. *Hydrological Processes*, *22*, 1–8. https://doi.org/10.1002/hyp6637.

Lehner, F., Coats, S., Stocker, T. F., Pendergrass, A. G., Sanderson, B. M., Raible, C. C., & Smerdon, J. E. (2017). Projected drought risk in 1.5 °C and 2 °C warmer climates. *Geophysical Research Letters*, *44*(14), 7419–7428.

Leketa, K., & Abiye, T. (2020). Investigating stable isotope effects and moisture trajectories for rainfall events in Johannesburg, South Africa. *Water SA*, *46*(3), 429–437. 10.17159/wsa/2020.v46.i3.8653.

Lelieveld, J., Hadjinicolaou, P., Kostopoulou, E., Chenoweth, J., et al. (2012). Climate change and impacts in the Eastern Mediterranean and the Middle East. *Climate Change*, *114*, 667–687.

Li, J., Pang, Z., Tian, L., Zhao, H., & Bai, G. (2022). Variations of stable isotopes in daily precipitation in a monsoon region. *Water*, *14*, 2891. https://doi.org/10.3390/w14182891.

Liotta, M., Bellissimo, S., Favara, R., & Valenza, M. (2008). Isotopic composition of single rain events in the Central Mediterranean. *Journal of Geophysical Research*, *113*, D16304.

Liu, Z., Bowen, G. J., & Welker, J. M. (2010). Atmospheric circulation is reflected in precipitation isotope gradients over the conterminous United States. *Journal of Geophysical Research*, *115*, D22120. https://doi.org/10.1029/2010JD014175.

Liu, J., Song, X., Fu, G., Liu, X., Zhang, Y., & Han, D. (2011). Precipitation isotope characteristics and climatic controls at a continental and an island site in Northeast Asia. *Climate Research*, *49*(1), 29–44.

Lucas, L. I., & Unterweger, M. P. (2000). Comprehensive review and critical evaluation of the half-life of tritium. *Journal of Research of the National Institute of Standards and Technology*, *105*(4), 541–549.

Mahindawansha, A., Jost, M., & Gassmann, M. (2022). Spatial and temporal variations of stable isotopes in precipitation in the mountainous region, North Hesse. *Water*, *14*, 3910. https://doi.org/10.3390/w14233910.

Majoube, M. (1971). Fractionation in O-18 between ice and water vapor. *Journal De Chimie Physique Et De Physico-Chimie Biologique*, *68*(4), 625–636.

Managave, S. R., Jani, R. A., NarayanaRao, T., Sunilkumar, K., Satheeshkumar, S., & Ramesh, R. (2016). Intra-event isotope and raindrop size data of tropical rain reveal effects concealed by event averaged data. *Climate Dynamics*, *47*(3–4), 981–987.

Mariotti, A., Pan, Y., Zeng, N., & Alessandri, A. (2015). Long-term climate change in the Mediterranean region in the midst of decadal variability. *Climate Dynamics*, *44*, 1437–1456.

Meslmani, Y., Faour, G., Fayad, A. (2010). *Climate-change Atlas of Syria: Technical report*. https://doi.org/10.13140/RG.2.2.26562.17601.

Mook, W.M.E. (2001). *Environmental isotopes in the hydrological cycle: Principles and applications. UNESCO/IAEA Series*.

Munksgaard, N. C., Wurster, C. M., Bass, A., & Bird, M. I. (2012). Extreme short-term stable isotope variability revealed by continuous rainwater analysis. *Hydrological Processes*, *26*(23), 3630–3634. https://doi.org/10.1002/hyp.9505.

Nir, A. (1967). Development of isotope methods applied to groundwater hydrology. In: *Proceeding of a symposium on isotope techniques in the hydrological cycle, Geophysical Monograph Series No. 11*. American Geophysical Union.

Önol, B., & Semazzi, F. H. M. (2009). Regionalization of climate change simulations over the Eastern Mediterranean. *Journal of Climate*, *22*, 1944–1961.

Ozturk, T., Ceber, Z.P., Türkeş, M., Kurnaz, M.L. (2015). Projections of climate change in the Mediterranean Basin by using downscaled global climate model outputs. *International Journal of Climatology*. https://doi.org/10.1002/joc.4285.

Petit, J. R., et al. (1999). Climate and atmospheric history of the past 420,000 years from the Vostok ice core, Antarctica. *Nature*, *399*, 429–436.

Pfahl, S., & Wernli, H. (2008). Air parcel trajectory analysis of stable isotopes in water vapor in the Eastern Mediterranean. *Journal of Geophysical Research*, *113*, D20104. https://doi.org/10.1029/2008JD009839.

Risi, C., Bony, S., & Vimeux, F. (2008). Influence of convective processes on the isotopic composition (δ^{18}O and δD) of precipitation and water vapor in the tropics: 2. Physical interpretation of the amount effect. *Journal of Geophysical Research*, *113*, D19306. https://doi.org/10.1029/2008JD009943.

Rozanski, K., Gonfiantini, R., & Araguas-Araguas, L. (1991). Tritium in the global atmosphere: Distribution patterns and recent trends. *Physical Geography*, *17*, S523–S536.

Rozanski, K., Araguas-Araguas, L., & Gonfiantini, R. (1992). Relation between long-term trends of oxygen-18 isotope composition of precipitation and climate. *Science*, *258*, 981–985. https://doi.org/10.1126/science.258.5084.981.

Rozanski, K., Araguás-Araguás, L., & Gonfiantini, R. (1993). Isotopic patterns in modern global precipitation. In P. K. Swart (Ed.), *Climate change in continental isotopic records. Geophysical Monograph Series No. 78, DC* (pp. 1–37). American Geophysical Union.

Sarker, M. H., Ahmed, S., Alam, Md. S., Begum, D., Kabir, T. N., et al. (2021). Development and forecasting drought indices using SPI (standardized precipitation index) for local level agricultural water management. *Atmospheric and Climate Sciences*, *11*, 32–52. https://doi.org/10.4236/acs.2021.111003.

Scholl, M. A., Shanley, J. B., Zegarra, J. P., & Coplen, T. B. (2009). The stable isotope amount effect: New insights from NEXRAD echo tops, Luquillo mountains, Puerto Rico. *Water Resource Research*, *45*, w12407. https://doi.org/10.1029/2008WR007515.

Smiatek, G., Kaspar, S., & Kunstmann, H. (2013). Hydrological climate change impact analysis for the Figeh Spring near Damascus, Syria. *Journal of Hydrometeorology*, *14*, 577–593.

Strong, M., Sharp, Z. D., & Gutzler, D. S. (2007). Diagnosing moisture transport using D/H ratios of water vapor. *Geophysical Research Letters*, *34*, L03404. https://doi.org/10.1029/2006GL028307.

Swart, P. K., Lohmann, J. A., McKenzie, J., & Savin, S. (1993). *Climate change in continental isotopic records. Geophysical Monograph Series No. 78, DC* (p. 374). American Geophysical Union.

Terzer, S., Wassenaar, L., Araguás-Araguás, L., & Aggarwal, P. (2013). Global isoscapes for δ^{18}O and δ^2H in precipitation: Improved prediction using regionalized climatic regression models. *Hydrology and Earth System Sciences*, *17*(11), 4713–4728. https://doi.org/10.5194/hess-17-4713-2013.

Terzer-Wassmuth, S., Wassenaar, L. I., Welker, J., & Araguas-Araguas, L. (2021). New high-resolution global and regionalized isoscapes of δ^{18}O, δ^2H, and d-excess in precipitation. *Hydrological Processes*, *35*(6), e14254.

Vystavna, Y., Matiatos, I., & Wassenaar, L. I. (2021). Temperature and precipitation effects on the isotopic composition of global precipitation reveal long-term climate dynamics. *Science Reporter*, *11*, 18503.

Yang, Q., Mu, H., Guo, J., Bao, X., & Martín, J. D. (2019). Temperature and rainfall amount effects on hydrogen and oxygen stable isotope in precipitation. *Quaternary International*, *519*, 25–31.

Yurtsever, Y., & Gat, J. (1981). Atmospheric waters. In J. R. Gat & R. Gonfiantini (Eds.), *Stable isotope hydrology: Deuterium and oxygen-18 in the water cycle. Technical Report Series No 210* (pp. 103–142). IAEA.

Zuber, A. (1986). Mathematical models for the interpretation of environmental radioisotopes in groundwater systems. In P. Fritz & J. C. Fontes (Eds.), *Handbook of environmental isotope geochemistry* (Vol. 2(B), pp. 1–59). Elsevier.

Publisher's Note

Springer Nature remains neutral with regard to jurisdictional claims in published maps and institutional affiliations.